Accurate Feature Extraction and Control Point Correction for Camera Calibration with a Mono-Plane Target

Y. Xiao
University of Edinburgh
yxiao@inf.ed.ac.uk

R.B. Fisher
University of Edinburgh
rbf@inf.ed.ac.uk

Abstract

The paper addresses two problems related to 3D camera calibration using a single mono-plane calibration target with circular control marks. The first problem is how to compute accurately the locations of the features (ellipses) in images of the target. Since the structure of the control marks is known beforehand, we propose to use a shape-specific searching technique to find the optimal locations of the features. Our experiments have shown this technique generates more accurate feature locations than the state-of-the-art ellipse extraction methods. The second problem is how to refine the control mark locations with unknown manufacturing errors. We demonstrate in a case study, where the control marks are laser printed on a A4 paper, that the manufacturing errors of the control marks can be compensated to a good extent so that the remaining calibration errors are reduced significantly.

1. Introduction

Recent years have seen the popularity of camera calibration using a mono-plane target (on which the control points are all coplanar). A mono-plane target can be economically made by just simply attaching a paper printed with identifiable marks (control marks) to a flat surface [1], offering great convenience for camera calibration in vision applications such as DVS (Desktop Vision System) [2]. However, the easy-to-use property of the mono-plane target should not compromise the accuracy of calibration. In this paper, we discuss issues related to how to improve calibration accuracy with a mono-plane target. Specifically we investigate two problems: 1) how to extract accurate features (projection of control marks) in images of the target and 2) how to obtain accurate locations of the actual control marks on the target, given unknown manufacturing errors. It is clear that a better calibration can be achieved if we have more accurate features and control marks.

The control marks on the calibration target used in this study are a 2D array of circles (Fig.1). Circular marks are commonly adopted for calibration targets [3]. Compared with checkerboard patterns, another popular category of control marks for calibration, circular marks offer at least the following advantages: 1) circular marks can be efficiently manufactured with good precision; 2) accuracy of ellipse (projection of circle) detection in images is arguably higher (for instance, [4] reports a 1/100 pixel level of ellipse detection accuracy, while corner detection from checkerboard images can achieve only about 1/10 pixel level of localization accuracy [17]); 3) the symmetry in shape of circles and ellipses can be used to improve significantly the accuracy of localization of the circles and ellipses, making them very "blur-resistant" (see Section 2.1); 4) the smoothness of circular/elliptical shapes allows the application of effective optimization techniques in searching for optimal locations of the circles/ellipses.

The projection of a circle is often an ellipse. In previous work, various ellipse detection techniques were used for calibration [4-8]. However, a majority of these methods extract ellipses individually in images without reference to the structure of the circles on the calibration target. We argue that such methodology may not be optimal for accurate feature extraction, since detection of a single ellipse can be vulnerable to image deficiencies such as noise, non-uniform illumination, etc. There are methods that map the entire structure of the control marks to the image planes and match them with real calibration images [9]. While seemingly more accurate, they suffer from modeling unknown factors in the imaging process such as illumination, surface reflectance, point-spread function of the lens, etc., degrading their performance in real world applications. In this paper, we propose a method that employs the structure of the control circles on the calibration target to guide the extraction of the corresponding ellipses in images. It still extracts each ellipse individually, however, the shape of the ellipse is constrained by the location and orientation of its corresponding circle on the calibration target, therefore potentially more accurate and reliable ellipse locations can be achieved.

The other problem studied in this paper is related to the locations of the control circles on the calibration target. Ideally the locations should be known beforehand. However, for the calibration target we used on which the

control circles are printed by a high-precision laser printer, we have found the minor offsets of the printed circle locations relative to their ideal locations contribute considerably to the overall residual calibration errors. We propose a method to compensate for the offsets based on the assumption that the offsets are caused by non-uniform paper loading speed by the printer. Our experiments support this hypothesis, and demonstrate that calibration errors are significantly reduced after the compensation.

While the paper is largely about 2D issues, camera intrinsic, extrinsic and lens distortion parameter estimation is fundamental to and is primarily seen in 3D contexts, where stereo cameras or light stripe triangulation systems depend on accurate camera calibration.

The remainder of the paper is organized as follows. Section 2 discusses the problem of ellipse extraction and Section 3 addresses the problem of circle location correction.

2. Feature extraction

2.1. Techniques

The control marks used for calibration in this study are circles. When a camera observes the calibration target, the circles on the target surface are projected to the image plane as ellipses (Fig.1). In order to calculate parameters of the camera, the locations of the ellipses in the images of the target are needed, which is usually done through ellipse extraction techniques.
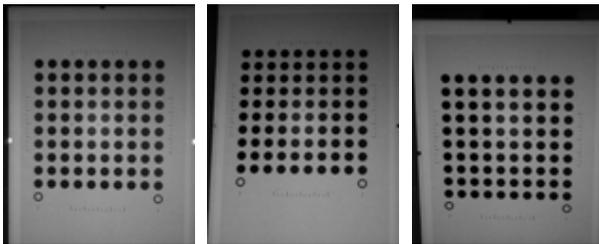
Figure 1: The calibration target at different views.

Ellipse extraction has a long history of study in computer vision with applications ranging from object recognition [5] to 3D reconstruction [6]. Early methods often take three steps: extract edge points, then use the Hough transform [10] to find points belonging to ellipses, and finally use ellipse fitting techniques [11] to obtain ellipse equations. Latest methods achieve subpixel accuracy in ellipse extraction by employing a template to compute subpixel edge locations [7] and using image gradients to derive additional curvature information [8]. While these methods are for general purpose, they are not necessarily optimal in the specific case of ellipse extraction for camera calibration.

First, the multi-step approach (image-edge-ellipse) employed in previous work does not have an overall measurement of the quality of extracted ellipses. Instead, each step introduces its own errors, allowing errors to propagate. Second, it is well known that edge detection and gradient calculation are sensitive to image deficiencies, which may render many extraction results invalid. Finally, the specific information about the calibration scene is not used. We argue that better ellipse extraction results can be achieved by exploiting the scene information and not separating ellipse extraction into multiple steps.

Look at the calibration scene in Fig.1. The circles are arranged in a 2D array. The radii of the circles and the distances between the circles are known. The background is a white paper and the foreground objects are solid black circles. In such a specific circumstance, it is quite possible that the scene information, e.g., the structure of the control circles and the background/foreground properties, can be used to assist ellipse extraction to achieve better accuracy and reliability. To this end, we devised a method to find optimal ellipse parameters from the target images directly, avoiding the problems with the previous multi-step approaches. The method maximizes the difference of intensity between the inside and outside of the ellipse, which provides a simple and yet effective measurement of the quality of ellipse extraction justified by the background/foreground property of the images. The metric structure of the control circles is used to initialize the optimization for the ellipse to avoid local minima.
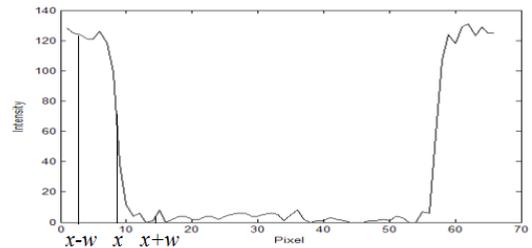
Figure 2: 1D profile of an ellipse from Fig. 1 and half points.

The graylevel properties of target images are illustrated in Fig. 2, where the 1D graylevel profile of an ellipse in Fig.1 is plotted. Ideally the profile should be a binary signal with a flat bottom and a flat top representing the foreground and background respectively, and a step edge between them representing the boundary of the ellipse. However, the real profile has a noisy top, noisy bottom and a few pixels of width in transition, due to various factors including illumination, imaging noise, image blur, etc. It is nontrivial to recover the true location of the edge (ellipse boundary) from a contaminated signal like Fig.2, especially when the models of illumination, image noise, and image blur are not

known. In this paper, we propose to use the half-points of the signal to capture the edge locations. A half point of a signal is the point where the signal has a graylevel value of the middle between the top and the bottom of the ideal binary signal. Since the ideal signal is usually unknown, we use the following formula to estimate a half point:

$$\arg\max_x \left(\left| \int_{x-\omega}^{x} g(u)du - \int_{x}^{x+\omega} g(u)du \right| \right) \quad (1)$$

where $g(u)$ denotes a graylevel signal, ω is a coefficient to define an integration window. The window should be set around an edge of the signal and not extend to the other edges. For the signal in Fig. 2, $\omega=5$ works sufficiently.

It is not difficult to prove that formula (1) gives the exact half point x if the signal is linearly interpolated between the top and the bottom. If it is not, our hypothesis is that formula (1) generates consistent systematic shifts on the edge locations and the shifts can be compensated when an ellipse is extracted as a whole with its boundary all satisfying formula (1) since shifts in opposite directions of the ellipse have opposite signs. The ellipse can then be estimated using the following formula:

$$\arg\max_{\mathbf{V}_C} \left(\left| \frac{1}{A_-} \iint_{\Omega_-} g(u,v)dudv - \frac{1}{A_+} \iint_{\Omega_+} g(u,v)dudv \right| \right) \quad (2)$$

In formula (2), Ω_+ denotes the region between the ellipse boundary C and its offset curve that is parallel to C with distance ω, and the area of Ω_+ is A_+. Similarly, Ω_- is the region between the ellipse boundary and its offset curve with distance -ω, and the area of Ω_- is A_-. $\mathbf{V}_C$ denotes the parameters of the ellipse C. In our implementation of the method proposed in this paper, the ellipse parameters are chosen as semi axes radii, ellipse orientation and ellipse center. The ellipse orientation is expressed by the angle between the major axis and the x-axis in the image coordinate frame.

By definition, formula (2) is equivalent to maximizing the difference of mean graylevel values between the inside and the outside of the ellipse. In principle, it is similar to the SUSAN edge detector [12]. The numerical approximation of formula (2) is as follows:

$$\arg\max_{\mathbf{V}_C} \sum_i \left| \sum_{j=-s\omega}^{0} g(\mathbf{x}_i + \frac{j}{s}\mathbf{n}_i) - \sum_{j=0}^{s\omega} g(\mathbf{x}_i + \frac{j}{s}\mathbf{n}_i) \right| \quad (3)$$

In formula (3), the integrals in formula (2) are turned to sums of graylevel values on grids in Ω_+ and Ω_-. The latitudes of the grids are parallel to the ellipse boundary C which is sampled at points $\mathbf{x}_i$, and the longitudes are

decided by $\mathbf{n}_i$ which are unit normal vectors of the ellipse boundary C at $\mathbf{x}_i$. s is used to adjust the sampling interval along a longitude. The graylevel values of the sampled points on the grids can be calculated from the original image using interpolation techniques [13]. Equation (3) can be optimized using the Simplex technique [14].

To ensure the optimization finds the correct ellipse boundary locations, it is important to initialize the ellipse parameters near the optimal solution. The initialization is done as follows. First a blob detection technique called BCoM (see details in the Section 2.2) is used to roughly estimate the ellipse centers, and then the camera is calibrated using the feature points, finally the parameters of the ellipses are obtained by projecting the circles on the calibration target to the image plane. It has been shown in our experiments that the BCoM is able to achieve subpixel accuracy in ellipse center extraction (some quantitative evaluation in Section 2.2), which serves well to provide initial estimate of the ellipse parameters.

2.2. Results

We carried out experiments to evaluate the ellipse extraction technique above. The first experiment is with synthetic data that was generated as follows. Five parameters: semi axes radii a and b, orientation ϕ, ellipse center u_0, v_0 were used to specify the geometry of an ellipse. The parameters were randomly chosen in the ranges $a \in [7, 13]$, $b \in [3, 7]$, $\phi \in [-\pi, \pi]$, and u_0, $v_0 \in [20,21]$. The graylevel value inside the ellipses is 150 and outside is 50. The images were first produced in higher resolution (410 by 410) and then smoothed using Gaussian filter with $\sigma = 10$, finally rescaled to resolution 41 by 41 and contaminated by additive Gaussian noise with $\sigma = 2$. 100 test images were generated.

The condition of synthesizing the ellipse images is the same as [4], in which two subpixel ellipse extraction methods: the moment preserving (MP) ellipse detector [7] and the moment and curvature preserving (MCP) detector [4] were tested and compared. The simulated images were used to test our maximizing outside-inside difference (MOID) ellipse extraction method, therefore we can make a fair comparison with the previous MP and MCP methods.

The parameters of MOID in this test were chosen as $\omega=3$ and $s= 0.1$. Since the blur kernel in synthetic data is Gaussian with $\sigma = 1$ (implemented in Gaussian with $\sigma = 10$ in the 10X enlarged images), $\omega=3$ proved a good balance between algorithm efficiency and accuracy in our experiments. Larger ω only produced negligible accuracy improvement with a increased computational cost linearly proportional to ω. Similarly, $s= 0.1$ was chosen empirically from a few trials of the MOID performance. With this setup

of parameters, the MOID detected all 100 ellipses in a time of 61.6563 seconds. Our implementation of the algorithm was written in Matlab script, and the computer is a windows PC with 2GB RAM and Intel Xeon 2.99 GHz CPU.

The comparison results are summarized in Table 1, where the RMS (root mean square) errors of the extracted ellipse centers are listed. It can be seen that our MOID method achieves higher precision in ellipse center extraction from the synthetic images than the MP and MCP methods, with about 20% and 10% improvement each.

The accuracy of the MOID method has also been tested in real calibration tasks. Table 3 reports the calibration results from ellipse centers using the MOID method for three stereovision systems. The reported measurements are described below. Each stereovision system has a pair of cameras of different type, as summarized in Table 2. Binary Center of Mass (BCoM) and Graylevel Center of Mass (GCoM) are also computed from the images to make comparison. The BCoM method computes the centroid of a blob (representing an ellipse) segmented from the original image (the technique is equivalent to computing the center of mass of the binary image of the blob). The segmentation is done by using Ostu's method [15]. The graylevel center of mass [10] is calculated on an image window which is expanded 10 pixels from the bounding box of the segmented blob. The BCoMs and GCoMs can be used as estimate to the centers of their underlying ellipses.

Table 1 RMS of detected ellipse centers

method	MP	MCP	MOID
x_0	0.0156	0.0137	0.0117
y_0	0.0150	0.0134	0.0121

Table 2 Specifications of the stereo systems evaluated

System	1	2	3
Camera Make	Mikrotron	Pulnix	Canon
Camera Type	Video B/W	Video B/W	Static Colour
Resolution	1280x1024	1392x1040	3456x2304
Lenses	75mm	35mm	58mm
Lighting	LED Panel	Diffusive	Flash
Baseline	Horizontal	Vertical	Horizontal

Table 3 Calibration errors using different feature extraction methods

		System 1	System 2	System 3
Reproj-ection	MOID	0.1094	0.0993	0.1755
	BCoM	0.1083	0.1160	0.1810
	GCoM	0.2632	0.1569	0.1951
Rectic ation	MOID	0.0843	0.0600	0.2494
	BCoM	0.1023	0.0813	0.2859
	GCoM	0.1778	0.0754	0.2612

The ellipse centers extracted by the three methods were used for calibration of the stereovision systems respectively. Once a calibration was done, two types of calibration errors were calculated to evaluate the quality of the calibration. The first calibration error is RMS of the calibration residuals (also known as reprojection errors). The other calibration error is the RMS of the vertical offsets of corresponding ellipse centers on the left and right images after stereo rectification. Ideally a pair of corresponding points on the left and right images can be rectified in such a way that only horizontal disparities exist. The rectification algorithms in [16] was chosen in this study since it minimizes image distortion after rectification. The vertical offsets between rectified corresponding points in real-world data are caused by the errors in the estimated epipolar geometry between the stereo cameras. The reprojection and rectification errors are two indicators to the accuracy of calibration of stereovision systems.

It can be seen that the MOID method consistently produces smaller calibration errors than the other two methods. GCoM produces noisy results especially in the LED lighting system (system 1) where the illumination is non-uniform, suggesting some sensitivity to lighting conditions. BCoM performs consistently as well in all the tests, but it generates larger calibration errors than MOID in most of the tests, especially rectification errors. The result suggests the MOID method is more accurate and precise than the other two methods.

3. Control point correction

When calibrating, the metric structure of the control marks (circles in this study) on the calibration target is often supposed to be accurate so that it can be used as "known" information to derive other parameters of the camera system. However, the precision of control marks comes with manufacturing cost, which may limit the achievement of high accuracy for a camera system. In this research, we proposed a method that can compensate for a fair amount of errors in the structure of control marks. Since the shifts between the real and ideal 3D coordinates of the control marks are fixed for a specific calibration target, our hypothesis is that they can be estimated and corrected using a sufficient number of observations.

Let us assume the location errors of control points are fixed and the location errors of feature points are i.i.d. Random. Then their relation can be expressed as below:

$$\mathbf{x}_{ji} = f_j(\mathbf{X}_i + \mathbf{\Delta}_i) + \mathbf{\delta}_{ji}, i = 1, \ldots, n, j = 1, \cdots, m \quad (4)$$

where f_j is the projection function of camera in the j-view, $\mathbf{X}_i$ are the ideal coordinates of the i-th control point, $\mathbf{x}_{ji}$ are the image coordinates of the feature point, $\mathbf{\Delta}_i$ are a

constant 3-vectors representing the shift of the control point, and $\boldsymbol{\delta}_{ji}$ is i.i.d 2D zero-mean white noise. Given this model, camera parameters and shifts of control points can be estimated by minimizing the following least squares error:

$$\underset{\mathbf{V},\boldsymbol{\Delta}_i}{\arg\min}(\sum_j \sum_i \left| f_j(\mathbf{X}_i + \boldsymbol{\Delta}_i) - \mathbf{x}_{ji} \right|^2) \qquad (5)$$

Formula (5) gives an unbiased estimate of the camera parameters $\mathbf{V}$ and the shift of the control point $\boldsymbol{\Delta}_i$ if the number of observations m is sufficient. However, if $\boldsymbol{\delta}_{ji}$ is not i.i.d random and m is small finite number, which is quite often the case in a real calibration task, systematic errors may occur in the calibration, and the errors will be partly reflected in the estimated $\boldsymbol{\Delta}_i$. This is the so-called overfitting problem.

Since $\boldsymbol{\delta}_{ji}$ may behave differently due to different conditions in the calibration tests such as illumination, image noise, etc., $\boldsymbol{\Delta}_i$ estimated using Formula (5) may not be consistent in all tests, which nevertheless will render the $\boldsymbol{\Delta}_i$ invalid. While realistically it is hard to devise a general method for estimating $\boldsymbol{\Delta}_i$ given unknown properties of $\boldsymbol{\delta}_{ji}$, extra constraints must be used to make the problem tractable. In the special case of this study, the calibration circles were printed on an A4 paper by a laserjet printer and then attached to a flat surface. We hypothesized the shifts of circles are caused by the non-uniform loading speed of the paper, therefore they only occur along the paper feeding direction (vertically on the A4 paper). The control points (centers of the control circles) form a 2D array where ideally a row of control points have the same vertical coordinate and a column of control points have the same horizontal coordinate. We assume the horizontal coordinates of the control points are unchanged (zero horizontal shift) and a row of control points are affected identically by the paper rolling speed and have the same shift in their vertical coordinate (identical vertical shift). With these assumptions, we only need to associate a variable representing a vertical shift to a row of control points rather than a translation vector to each individual control point. Then Formula (5) can be re-written as:

$$\underset{\mathbf{V},\boldsymbol{\Delta}_i}{\arg\min}(\sum_j \sum_i \sum_k \left| f_j(\mathbf{X}_{ik} + \boldsymbol{\Delta}_i) - \mathbf{x}_{jik} \right|^2) \qquad (6)$$

The indices j,i,k in Formula (6) are used to denote j-view of the calibration target, i-row and k-column of the control points. It is clear that problem (6) has less degree of freedom (number of parameters) than problem (5), and therefore is potentially able to generate more reliable results. Even

though the overfitting problem may still exist, its influence has been alleviated.

(a)　　　　　　　　(b)

(c)　　　　　　　　(d)
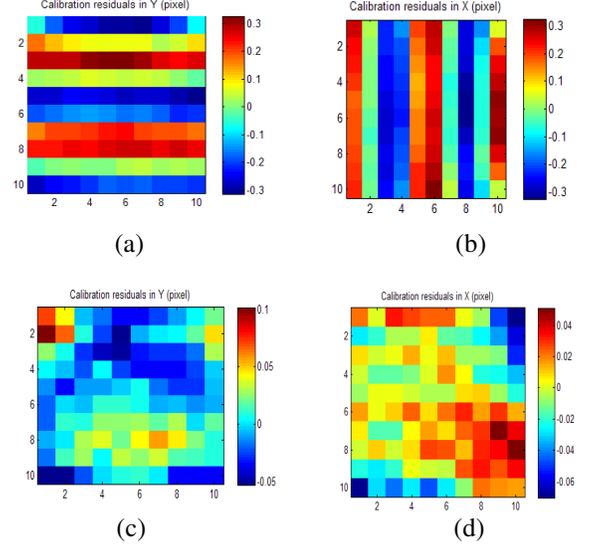
Figure 3: Calibration residuals for control points of the target in Fig 1. Before control point correction: (a) y-residuals when target was placed in normal orientation as in Fig. 1; (b) x-residuals when target was placed in orientation 90° to Fig. 1. After control point correction: (c) y-residuals for the calibration data in (a); y-residuals for the calibration data in (b).

Our experiments show the zero-horizontal-shift and identical-vertical-shift assumptions are valid. First, we calibrated a camera using the calibration target placed in normal orientation as in Fig. 1, and we obtained a calibration residual map as in Fig.3(a). Horizontal stripe patterns appeared in the residuals in y-coordinate, which indicates that a row of control points have similar vertical shifts on the target plane. When we rotated the target by 90° and used it to calibrate the same camera again, we obtained vertical stripe patterns in x-residuals of the calibration. This can be explained as the vertical shifts of control points have been turned to horizontal due to the 90° rotation of the target. Second, we have estimated the vertical offsets of the control point rows from different sets of calibration images of the same target from 3 different cameras. Fig. 4 depicts the vertical shifts of 10 rows of control points for the calibration target in Fig. 1 estimated from 5 frames of images acquired from the left and right cameras of stereo system 1 (Cam 1F and Cam 1R) and the top and bottom cameras of stereo system 2 (Cam 2T and Cam 2B) mentioned in Table 2. It can be seen that the vertical shifts are consistent across the cameras and stereo systems, which supports the validity of the zero-horizontal-shift and the identical-vertical-shift assumptions about the control circles. In the meantime, the results also demonstrate that

the degree of overfitting for each estimate of the vertical shifts is not severe. We hypothesize that the unknown errors of feature point locations have behaved relatively randomly for each row of control points and therefore been compensated well in solving problem (6). Since the variation of the vertical shifts for each row of control points is not large, we calculate their mean value and use it to correct the coordinates of the control points of that row. After the control point correction, we can use the new control point coordinates for camera calibration.

Fig.3(c,d) illustrate the calibration residual maps using the corrected control point positions. The image feature data are the same as those in Fig.3(a,b) respectively. It can be seen that Fig.3(c,d) do not have the stripe patterns in Fig.3(a,b), and also the magnitude of residuals in Fig.3(c,d) is significantly reduced, indicating that the systematic drift of the control points have been compensated effectively. Note that the residual maps in Fig.3(c,d) are still not completely spatial-random, which suggests that there may be still some other sources of systematic error in the calibration process, e.g., unknown illumination.
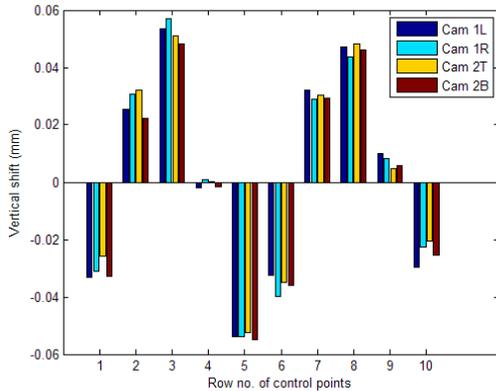
Figure 4: Estimated vertical shifts of control points for the calibration target in Fig. 1.

Table 4 Calibration errors before and after control point correction (in pixels)

		System 1	System 2	System 3
Reproj-ection	before	0.1628	0.1817	0.2789
	after	0.1094	0.0993	0.1755
Rectific-ation	before	0.0825	0.0714	0.2813
	after	0.0843	0.0600	0.2494

We verified the corrected control point coordinates in new camera calibration applications. The calibration errors listed in Table 3 are the results of calibration using the corrected control point coordinates for all 3 algorithms. The results using uncorrected control point coordinates are compared in Table 4. The MOID ellipse extraction method

was chosen to acquire feature points since the MOID method has been proved accurate. It can be seen that the correction of the control point coordinates significantly reduced the calibration errors (especially the re-projection errors) despite the difference in camera types, lighting conditions, and stereo configurations. It also shows that a small amount of location compensation (0.05 mm maximum in Fig. 4) can significantly reduce calibration errors and improve calibration accuracy.

4. Conclusion

This paper has reported our study on two issues related to camera calibration, namely, how to achieve accurate features and how to obtain accurate control points. It has been shown that more accurate feature extraction can be done by employing the information of the metric structure of the control marks and integrating the multiple steps of feature extraction to a single optimization framework. The objective function of the optimization, namely, the difference between the inside and outside of the features has been proved valid.

For 3D locations of control points, it is demonstrated that the offsets between ideal locations and real locations can be estimated by hypothesizing correctly the cause of the offsets. In this particular case of study, it has been shown that the location errors occurred mainly on vertical direction. A correction of the control point locations is done to effectively improve calibration performance.

The principles in the feature extraction and control point correction in this paper may be easily extended to other types of control marks and calibration targets.

References

[1] B. Triggs, "Autocalibration from Planar Scenes", *Proc. European Conf. Computer Vision,* pp. 89–105, Freiburg, Germany, June 1998.

[2] Z. Zhang, "A Flexible New Technique for Camera Calibration", *IEEE Trans. Pattern Analysis and Machine Intelligence*, vol. 22, no. 11, pp. 1330-1334, 2000, doi:10.1109/34.888718.

[3] J. Heikkila, "Geometric Camera Calibration Using Circular Control Points", *IEEE Trans. Pattern Analysis and Machine Intelligence*, vol. 22, no. 10, pp. 1066-1077, 2000, doi:10.1109/34.888718.

[4] J. Heikkila, "Moment and Curvature Preserving Technique for Accurate Ellipse Boundary Detection", *Proc. Int. Conf. Pattern Recognition,(ICPR '98)*, pp. 734-738, vol. 1, 1998.

[5] E.R. Davies, "Finding Ellipses Using Generalised Hough transform", *Pattern Recognition Letters*, vol. 9, no. 2, pp. 87-96, 1989f.

[6] L. Quan, "Conic Reconstruction and Correspondence from Two Views", *IEEE Trans. Pattern Analysis and Machine*

Intelligence, vol. 18, no. 2, pp. 151-160, 1996, doi:10.1109/34.481540.

[7] A.J. Tabatabai, O.R. Mitchell, "Edge Location to Subpixel Values in Digital Imagery", *IEEE Trans. Pattern Analysis and Machine Intelligence*, vol. 6, no. 2, pp. 188-201, 1984.

[8] J-N Ouellet, P. Hebert, "Precise Ellipse Estimation without Contour Point Extraction", Machine Vision Applications, vol. 21, no. 1, pp. 59-67, 2009, doi:10.1007/s00138-008-0141-3.

[9] D. Douxchamps, K. Chihara, "High-Accuracy and Robust Localization of Large Control Markers for Geometric Camera Calibration",*IEEE Trans. Pattern Analysis and Machine Intelligence*, vol. 31, no. 2, pp. 376-383, 2009.

[10] R.M. Haralick, L.G. Shapiro, *Computer and Robot Vision*, Addison-Wesley, 1992.

[11] A. W. Fitzgibbon, M. Pilu, R. B. Fisher, "Direct Least Squares Fitting of Ellipses", *IEEE Trans. Pattern Analysis and Machine Intelligence*, vol. 21, no. 5, pp. 476-480, 1999.

[12] S.M. Smith, J.M. Brady, "SUSAN – a New Approach to Low Level Image Processing", *International Journal of Computer Vision*, vol. 23, no. 1, pp. 45-78, 1997.

[13] R.C. Gonzalez, R.E. Woods, "Digital Image Processing", 2nd Ed. 2002, Prentice Hall.

[14] J.A. Nelder, R. Mead, "A Simplex Method for Function Minimization," *The Computer Journal*, vol. 7, pp. 308-313, 1968.

[15] N. Ostu, "A Threshold Selection Method from Gray-level Histograms", *IEEE Trans. Syst. Man and Cybern.*, vol. 9, no. 1, pp. 62-66, 1979.

[16] A. Fusiello, E. Trucco, and A. Verri, "A Compact Algortihm for Rectification of Stereo pairs", Machine Vision and Applications, vol. 12, no. 1, pp. 16-22, 2000.

[17] http://www.vision.caltech.edu/bouguetj/calib_doc/htmls/example.html